JVST A
Journal of Vacuum Science & Technology A

Phosphites as precursors in atomic layer deposition thin film synthesis

Cite as: J. Vac. Sci. Technol. A **39**, 032404 (2021); https://doi.org/10.1116/6.0000844
Submitted: 07 December 2020 • Accepted: 16 February 2021 • Published Online: 08 March 2021

Kristian B. Kvamme, Amund Ruud, Kristian Weibye, et al.

JVST A
Journal of Vacuum Science & Technology A

ARTICLE

avs.scitation.org/journal/jva

Phosphites as precursors in atomic layer deposition thin film synthesis

Cite as: J. Vac. Sci. Technol. A **39**, 032404 (2021); doi: 10.1116/6.0000844
Submitted: 7 December 2020 · Accepted: 16 February 2021 ·
Published Online: 8 March 2021

Kristian B. Kvamme,[1,a)] Amund Ruud,[1] Kristian Weibye,[1] Timo Sajavaara,[2] and Ola Nilsen[1,b)]

AFFILIATIONS

[1]Department of Chemistry, Centre for Materials Science and Nanotechnology, University of Oslo, P.O. Box 1033, Blindern, N-0315 Oslo, Norway
[2]Department of Physics, University of Jyväskylä, P.O. Box 35, Jyväskylä FIN-40014, Finland

Note: This paper is part of the 2021 Special Topic Collection on Atomic Layer Deposition (ALD).
[a)]**Electronic mail:** k.b.kvamme@smn.uio.no
[b)]**Electronic mail:** ola.nilsen@kjemi.uio.no

ABSTRACT

We here demonstrate a new route for deposition of phosphorous based materials by atomic layer deposition (ALD) using the phosphites Me_3PO_3 or Et_3PO_3 as precursors. These contain phosphorous in the oxidation state (III) and are open for deposition of reduced phases by ALD. We have investigated their applicability for the synthesis of LiPO and AlPO materials and characterized their growth by means of *in situ* quartz crystal microbalance. Phosphites are good alternatives to the established phosphate-based synthesis routes as they have high vapor pressure and are compatible with water as a coreactant during deposition. The deposited materials have been characterized using XPS, x-ray fluorescence, and ion beam analysis for composition analysis, spectroscopic ellipsometry for thickness, and FTIR for local structure.

I. INTRODUCTION

Phosphate materials have the ability to form redox inactive polymeric structures of polyanions with lithium as a charge compensating cation. Polyanions consist of phosphorus tetrahedrally coordinated by oxygen, sulfur, or nitrogen. They may form monomers or polymeric structures with varying lengths and readily form amorphous materials. When combined with aluminum in a near equal ratio, they can form complex porous structures resembling zeolites, also known as AlPO materials.[1] Similar structures may also be formed from polyanions such as silicates, sulfates, borates, and even transition element polyanions such as vanadates, molybdates, niobates, and many more.[2] The interactions between the polyanion and the charge compensating cation, Li in LiPON or Fe in $FePO_4$, will be affected by the covalent character of the polyanion itself. This can be controlled by the choice of central atom, here phosphorus, and its coordinates. When oxygen is substituted for nitrogen as a coordinate atom, the overall covalent character of the polyanion is increased. This effect is utilized in the formation of the LiPON structure. An alternative to substituting the coordinate atoms is altering the oxidation state of the central atom. A reduction of the oxidation state of phosphorous from +V to +III will result in an increased covalent character of the polyanion toward the cation, with the resulting shift in electrochemical potential due to inductive effects.[3] Various phosphates have been thoroughly studied, but phosphites are rarely investigated. Phosphites also form polyanionic tetrahedral structures that tend to polymerize into asymmetric polyhedral superstructures. Three of the vertices in the phosphite bond to electronegative elements such as oxygen, while the remaining may bond directly to hydrogen, such as in phosphite acid, or occupy nonbonding electrons, such as for the phosphite precursors used in this study.

Phosphates are reported to be biocompatible, such as for apatitesm,[4] potential proton conductors (Ca:$LaPO_4$),[5] gate dielectrics (certain stoichiometries of aluminum phosphates),[6] and as hosts for luminescent materials (titanium phosphates).[7] We have used atomic layer deposition (ALD) to produce the films presented in this work.[8] The ALD technique is advantageous in that uniform thin films can be deposited on flat as well as structured surfaces with atomic level thickness control. The films are grown using

sequential self-limiting reactions between a reactant in the gas phase and active sites on the substrate surface. The process is relatively mild in that deposition temperatures are low enough to avoid thermal decomposition of the reactants and its products. This opens for the application of exploratory chemistry, such as the phosphites used here.

$POCl_3$, P_2O_5, and Me_3PO_4 have previously been used as phosphate precursors in ALD,[9,10] where P_2O_5 was the first reported precursor.[10] In that work, the deposition was performed at temperatures above 400 °C where a high degree of decomposition of the precursor is likely to take place, hampering the self-limiting growth aspect of ALD. $POCl_3$ is a good phosphate precursor and does not require ozone as an oxygen source.[11] This is a major advantage when depositing on large structured substrates due to possible ozone depletion from catalytic decomposition with the substrate,[12] as well as the fact that ozone can oxidize other components in the film, thus hampering the deposition of reduced phases. The main drawback of $POCl_3$ is chlorine and its possible contaminations in the deposited film.[13] For deposition of lithium containing compounds, the formation of stable LiCl is expected. Me_3PO_4 is the current primary choice of phosphate precursor in ALD, showing uniform growth and compatibility with several ALD systems.[5,7,9,13–15] Furthermore, the phosphate content in the film can be tuned to above 60 at. %.[15] Our approach is the deposition of phosphorous based films using precursors where phosphorous is in the +III oxidation state, namely, trimethyl phosphite (Me_3PO_3) and triethyl phosphite (Et_3PO_3). These precursors will replace trimethyl phosphate (Me_3PO_4) in the established deposition routes for aluminum phosphate ($AlPO_4$)[13] and lithium phosphate (Li_3PO_4)[9,16] by ALD.

II. EXPERIMENT

All deposition experiments were performed using an F-120 SAT hot wall ALD reactor (ASM Microchemistry Ltd.). The precursors used are listed in Table I. Li-O^{t}Bu was kept at a source temperature of 130 °C, while all the other precursors were kept in external bubblers at room temperature. Me_3PO_3 has a flash point of 28 °C inferring extra safety precautions such as using external steel bubblers. The high vapor pressure of 23 mbar means that there is no need for an additional carrier gas or additional heating of the precursor. This is in contrast to the currently used Me_3PO_4, which has a notably lower vapor pressure (1.1 mbar) and needs the aforementioned measures. The pulse and purge times were kept constant for the precursors not under investigation. Table I also shows the experimental pulse and purge times. $POCl_3$ was used as the phosphate precursor for the XPS reference experiments and Me_3PO_4 was used for the FTIR reference experiments. The reference experiments were also deposited by ALD.

TABLE I. Precursors and pulse parameters for phosphite synthesis.

Precursor	CAS	Pulse (s)	Purge (s)
Me_3PO_3 (99%, Sigma-Aldrich)	121-45-9	2	3
Me_3PO_4 (97%, Sigma-Aldrich)	512-56-1	3	4
Et_3PO_3 (98%, Sigma-Aldrich)	122-52-1	2	3
LiO^{t}Bu (97%, Sigma-Aldrich)	1907-33-1	5	2
$AlMe_3$ (99%, Sigma-Aldrich)	75-24-1	0.5	2
H_2O (>10 MΩ)	—	0.5	2
O_3	—	3	3

N_2 carrier gas was generated with an N_2 generator [Schmidlin-Sirroco 5 (99.999% Ar + N_2)]. The gas was further purified by a Mykrolis purifier before entering the reactor, keeping O_2 and H_2O levels below 1 ppm. Ozone was generated using an O_3-generator (InUSA-AC2025) supplied with O_2 (99.5% O_2, AGA) generating a flow rate around 500 cm^3 min^{-1} when pulsing. The reactor pressure was kept between 3.0 and 3.6 mbar during deposition with a total N_2 flow of 500 cm^3 min^{-1}. Si(111) substrates were used. Thickness and refractive index (at 632.8 nm) was measured by spectroscopic ellipsometry using a wavelength range of 380–900 nm (Woollam alpha-SE, COMPLETEEASE software). An in-house designed crystal holder was used for quartz crystal microbalance (QCM) analysis, measured using a Maxtex TM400 unit and a PLO-10i oscillator. QCM was used to study the growth rates and saturation by relating the frequency response to mass change through the Sauerbrey equation calibrating the response with a known internal standard (TMA + H_2O).[17] A pulse cycle is repeated 20 times and the average response and standard deviation of the 16 middle replicates are reported. XPS analysis was performed on a theta probe angle-resolved x-ray photoelectron spectrometer (Thermo Scientific). XPS analysis was performed on the surface layer, without sputtering. X-ray fluorescence (XRF) analysis was performed on a PANalytical Axios mAX mineral spectrometer and interpreted with the OMNIAN AND STRATOS analysis software. Time-of-flight elastic recoil detection analysis (TOF-ERDA) was done using 10.2 MeV $^{63}Cu^{5+}$ ions.[18]

III. RESULTS AND DISCUSSION

The two phosphite precursors (Me_3PO_3 and Et_3PO_3) were investigated as possible candidates for ALD deposition by first attempting to deposit lithium phosphite (LiPO). The initial QCM analysis showed slight differences for the two precursors, particularly for the phosphite response, at 60 s in Fig. 1. Et_3PO_3 seems to reach saturation around the end of the pulse, while the Me_3PO_3 pulse has a high mass change throughout the pulse followed by a large mass loss during the following purge. This may be an indication of reaction with absorbed water into the bulk of the film from the water pulse, as similarly reported for LiOH deposited by ALD.[19] In addition, the total mass change of the Me_3PO_3 subcycle is significantly larger than that of the Et_3PO_3 subcycle. We also discovered that an oxygen source was required to obtain films for both phosphite precursors. Deposition attempts using only alternating pulsing of the phosphite precursors and the cation precursor gave no film. This is in accordance with the Me_3PO_4 subcycle, which also gives no film without a cation subcycle.[15] Water and ozone were tested as oxygen sources after the phosphite precursor pulse, both individually and in combination. We concluded that a water pulse after each precursor pulse resulted in a stable product. In addition, using only water was viewed as beneficial compared to

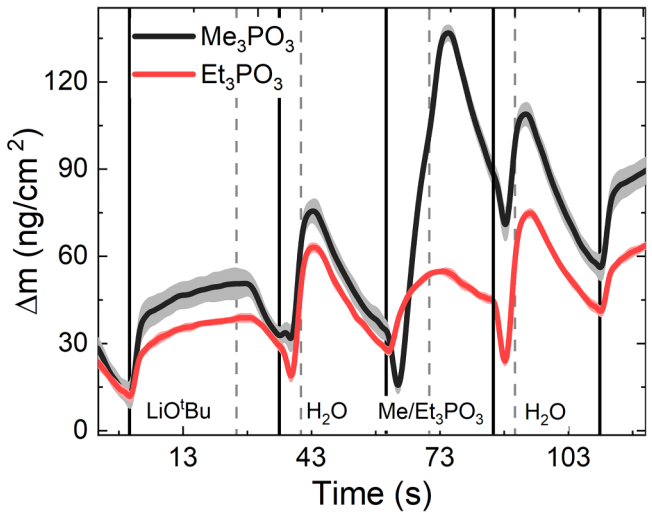

FIG. 1. QCM reactivity analysis of the LiPO systems. The results are shown as mass change per area as a function of elapsed time. The centerline is the average over ten subsequent cycles with the shaded area representing the standard deviation. The solid vertical lines indicate pulse start, and the dashed vertical lines indicate pulse stop. The deposition was performed at 225 °C and the pulsing sequence for both experiments are 25 s LiO^tBu, 10 s purge, 5 s H_2O pulse, 20 s purge, 10 s Me_3PO_3/Et_3PO_3, 15 s purge, 5 s H_2O pulse, and 20 s purge.

ozone as it reduces the probability of oxidizing the phosphite groups to phosphate.

The Et_3PO_3 process is unstable and shows large thickness gradients on the deposited films in the temperature range 175–250 °C. Furthermore, Et_3PO_3 films with thicknesses of 50 nm or more were slightly opaque. This behavior is also observed in ALD films with high Li_2CO_3 and LiOH content,[20] which is the probable product if no phosphorous is incorporated into the film.[20] This assumption was confirmed by XPS, where the phosphorous content when using the Et_3PO_3 precursor never exceeded 2%. From here on, we will focus on the results using Me_3PO_3 as the phosphite precursor, as this was the only precursor that gave satisfactory products. From the QCM analysis, a 2/3 s pulse/purge on the Me_3PO_3 subcycle was found sufficient for saturative growth on Si substrates. The remaining pulse and purge parameters are given in Table I. The temperature window for the LiPO system was found by depositing in the temperature range 150–250 °C, as shown in Fig. 2. The error bars in Fig. 2 represent the standard deviation of ellipsometric analysis of seven points throughout the reaction chamber. At 225 °C, the product is consistent throughout the reaction chamber, as shown with the narrow error bars for both refractive index and growth rate at that temperature for Me_3PO_3. The refractive index has a plateau in the range of 150–225 °C, indicating a consistent product in that temperature range. The growth rate goes through a maximum at 175 °C and decreasing as the temperature is increased. The Me_3PO_3 process gives uniform films in the thickness range tested, and the growth rate stabilizes after around 600 ALD cycles, as indicated by Fig. 3. The variation in refractive index with film thickness for these films, with a drop in refractive index at 300 supercycles (Fig. 3) may be related to a growth mechanism where islets form and grow into structured shapes with apparent lower density before these grow together and reach a stable density.[21] The surface roughness is further studied using AFM later in the article.

Aluminum phosphite (AlPO) was deposited using Me_3PO_3 as the phosphite precursor based on the performance of the precursors in the LiPO process. An initial QCM reactivity analysis was

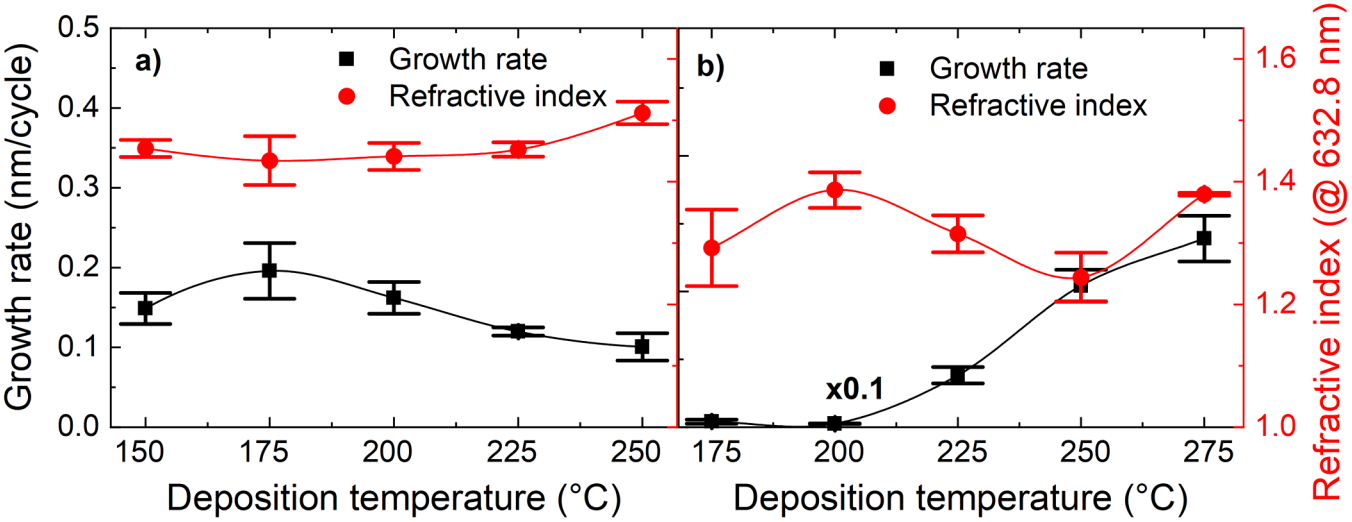

FIG. 2. Growth rate (nm/cycle) (left) and refractive index (at 632.8 nm) (right) as a function of temperature for the deposition of LiPO thin films on Si substrates using Me_3PO_3 precursor (A) and Et_3PO_3 precursor (B). The growth rate of the Et_3PO_3 is divided by ten for clarity, as indicated in the figure. The pulsing sequence is 5 s LiO^tBu, 2 s purge, 0.25 s H_2O pulse, 2 s purge, 2 s Me_3PO_3/Et_3PO_3, 3 s purge, 0.25 s H_2O pulse, 2 s purge, and 250 cycles.

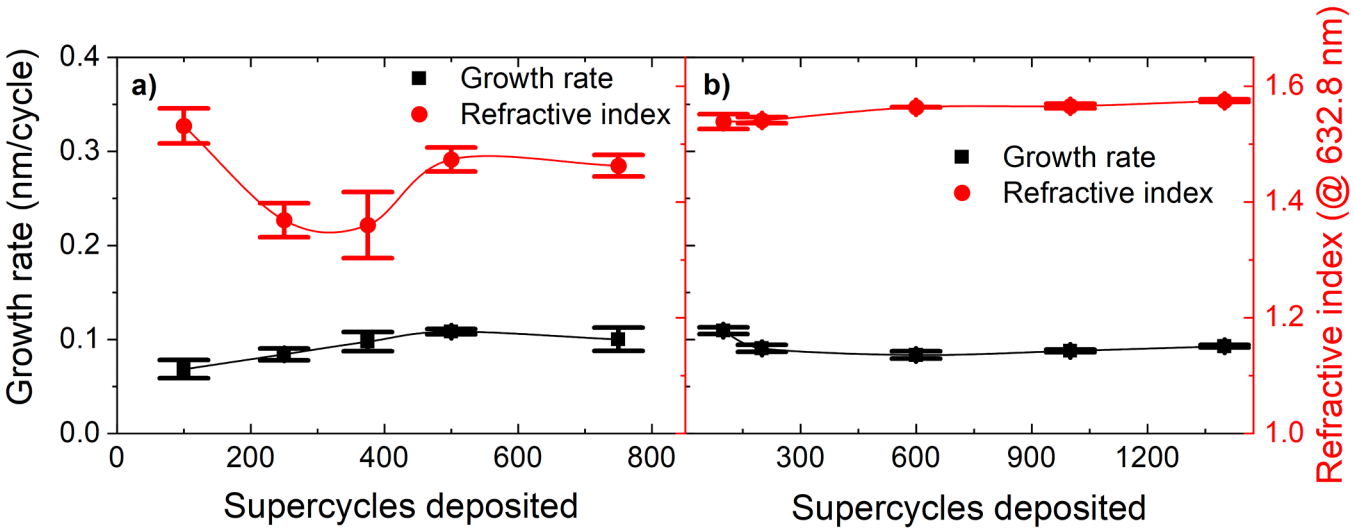

FIG. 3. Growth rate and refractive index as a function of film thickness for LiPO and AlPO. The refractive index of the LiPO films was challenging to determine with good certainty due to film roughness.

performed, and the phosphite response is very similar to what was previously seen for LiPO using the same precursor (Fig. 4). The pulse parameters for the phosphite precursor were set to the same value as for LiPO, due to the converging results. The TMA pulse and purge were set based on prior experience with this precursor in the same ALD reactor.

The stability window was determined by depositing film as a function of temperature in the range of 175–275 °C (Fig. 5). A slight decrease in the growth rate is observed with the increasing temperature. This is expected due to a decrease of the density of reactive sites with the increasing temperature.[22] The refractive index remains almost constant and gives an indication of a stable

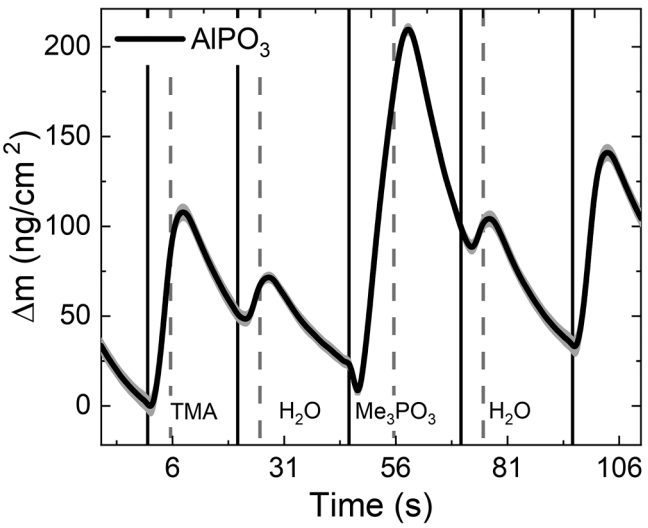

FIG. 4. QCM reactivity analysis for the AlPO system using a pulsing scheme of 5 s $AlMe_3$, 15 s purge, 2.5 s H_2O pulse, 20 s purge, 10 s Me_3PO_3, 15 s purge, 2.5 s H_2O pulse, and 20 s purge at a deposition temperature of 225 °C. The black line is the average over 10 subsequent AlPO supercycles, and the gray area is the standard deviation. Solid vertical lines indicate pulse start, and vertical dashed lines indicate purge start.

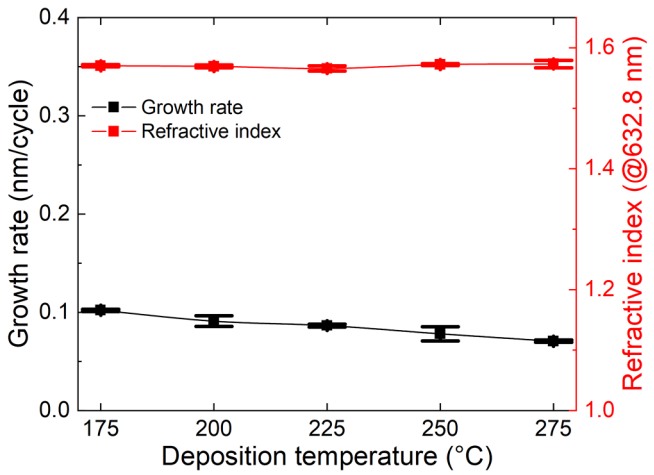

FIG. 5. Growth rate and refractive index of AlPO films as a function of deposition temperature using 1000 cycles of the pulsing scheme 0.5 s $AlMe_3$, 3 s purge, 0.5 s H_2O pulse, 2 s purge, 2 s Me_3PO_3, 3 s purge, 0.5 s H_2O pulse, and 2 s purge.

TABLE II. TOF-ERDA and XPS results of atomic concentrations at the surface layer of the analyzed films. The uncertainties in the XPS analysis are not posted but are significantly larger than for the TOF-ERDA results.

Measurement method	Product	%at P	%at O	%at C	%at M	%at H	M:P:O
Al_yPO_x					M = Al		
TOF-ERDA	AlPO (Me_3PO_3) 9:1	7.8 ± 0.5	55.2 ± 2	1.9 ± 0.2	21 ± 1	15 ± 2	4.2:1:11
XPS	AlPO (Me_3PO_3) 9:1	9.0	49.8	21.7	19.5		2.2:1:5.5
XPS	AlPO (Me_3PO_3) 1:1	5.5	47.1	24.2	23.2		4.2:1:8.5
XPS	AlPO ($POCl_3$)	6.9	51.8	21.6	18.4	1.3	2.7:1:7.5
Li_yPO_x					M = Li		
TOF-ERDA	LiPO (Me_3PO_3)	11 ± 2	51 ± 2	1.2 ± 0.4	35 ± 2	<1.5	3.1:1:4.6
XPS	LiPO (Me_3PO_3)	9.1	41.9	18.1	30.8		3.4:1:4.6
XPS	LiPO (Et_3PO_3)	0	42.4	26.6	31.0		—

process throughout the temperature range. Slight gradients were seen at the substrate edges at high temperatures, which could indicate that the Me_3PO_3 precursor starts to decompose. The growth as function of deposition cycles is given in Fig. 3 and shows a relatively constant growth rate with thickness at 0.1 nm/cycle.

ALPO elemental composition was analyzed using TOF-ERDA (Table II). The AlPO system was further used as a model to determine whether the composition of the product could be controlled by changing the subcycle composition, as the aluminum to phosphorous ratio of the AlPO films could be measured using a simpler elemental characterization procedure, XRF (Fig. 6). This was done by changing the relative number of TMA and Me_3PO_3 subcycles pulsed from 10% to 90% Me_3PO_3 and determining the composition by XRF (Fig. 7). In addition to determining at what level the composition of the product can be controlled, reaction stability analysis was performed using QCM and spectroscopic ellipsometry. Both methods show complimentary trends with respect to the growth rate with changing subcycle composition. The growth rate is the highest for pure TMA + H_2O cycles. When the subcycle ratio is around 1:1, there is a plateau of relatively constant growth rates before the growth rate again decreases for excess Me_3PO_3 subcycles. Uniform films were produced at all the compositions tested apart from when only Me_3PO_3 + H_2O was pulsed, where no film was formed, as expected. The phosphorous concentration in the films increases linearly with the phosphite subcycle content in the range of 10%–90% Me_3PO_3 pulsed, with a maxima of 25% phosphorous at 90% Me_3PO_3 pulsed [Fig. 7(a)]. The phosphorous content increases with increasing deposition temperature, until the concentration saturates at 25% phosphorous at 225 °C [Fig. 7(b)].

X-ray photoelectron spectroscopy (XPS) was used to quantify the composition and oxidation states of the components of selected AlPO and LiPO films. The results from the quantification are shown in Table II. The carbon content of the measured films was surprisingly high when measured by XPS, requiring further

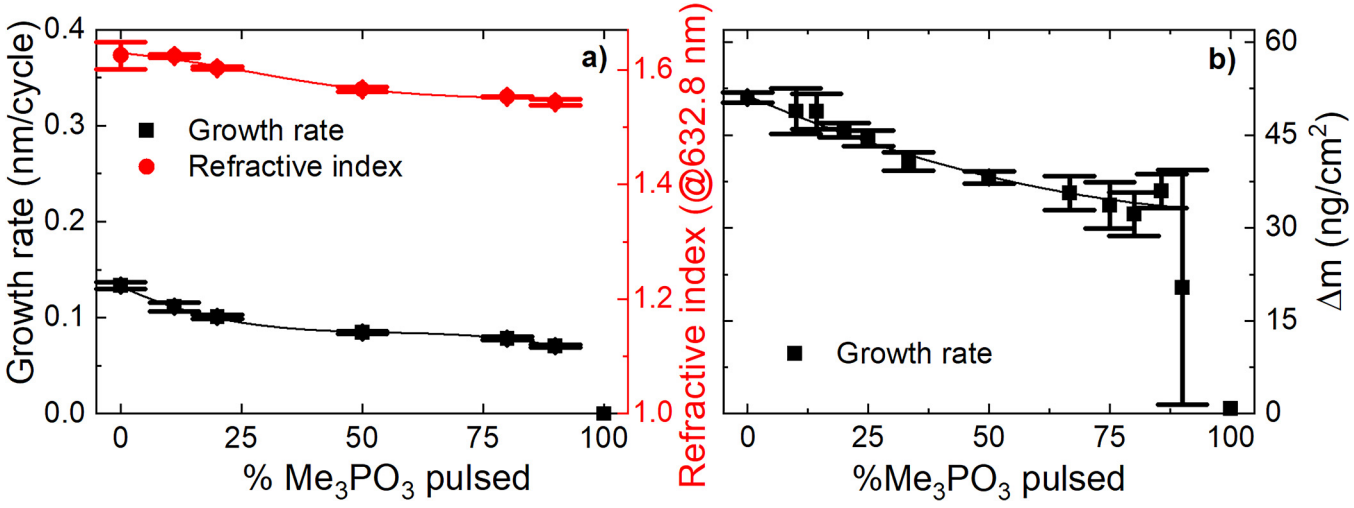

FIG. 6. Change in growth rate of the AlPO system when the amount of Me_3PO_3 subcycles relative to the amount of TMA subcycles is varied. Measured by spectroscopic ellipsometry (a) and QCM (b).

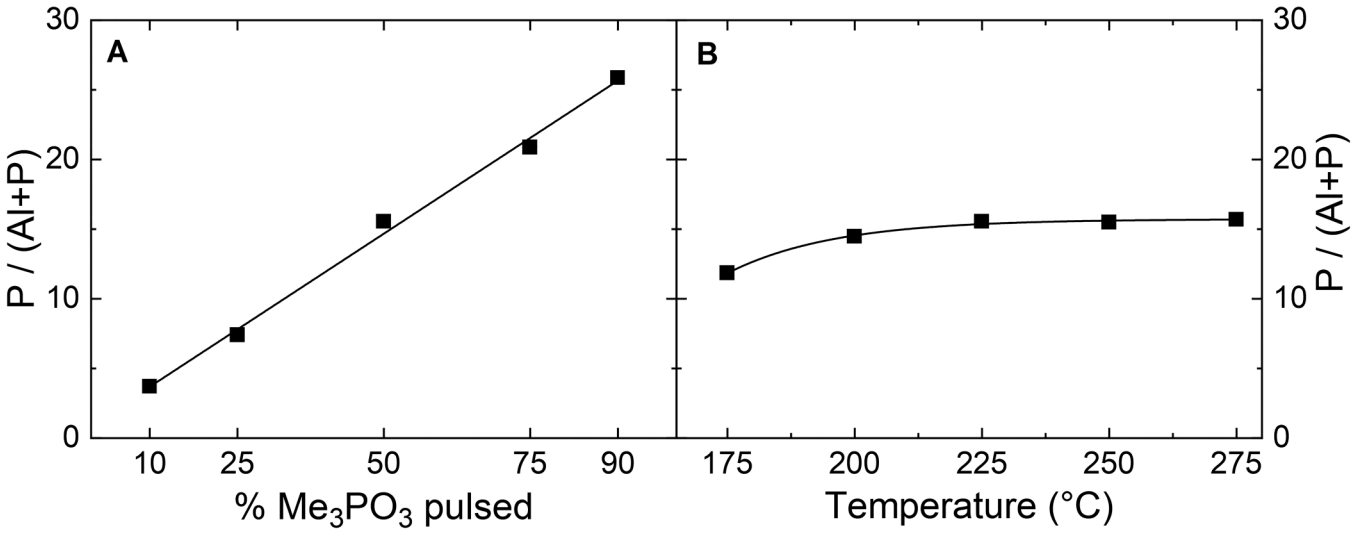

FIG. 7. XRF measurements of composition. (a) relates the change in phosphorous content of the deposited AlPO films when changing the relative amount of Me_3PO_3 and TMA subcycles at 225 °C. The temperature dependence of phosphorous concentration is shown in (b) for 50% Me_3PO_3 pulsed.

investigations. Selection of the films was analyzed with TOF-ERDA to get an accurate composition of the entire film. TOF-ERDA gives quantitative composition throughout the film, whereas XPS is only surface sensitive when sputtering is not used.[23] It should also be noted that sputtering in XPS can alter the lithium composition of the investigated film. TOF-ERDA analysis confirmed that the carbon detected by XPS was mainly located at the surface and we consider it to be contamination from handling the samples in air after deposition. XPS analysis shows a P2p 3/2 binding energy in LiPO at 133.0 eV. This is 0.6 eV lower than what reported for P(V) Li_3PO_4 by Kozen *et al.*[24] The P(V) $LiPO_3$ P2p peak has previously been reported at 134.5 eV by Chowdari *et al.*[25] P(V) $AlPO_4$ P2p has been reported at 134.4 eV.[26] This is the same as the measured binding energy for $AlPO_4$ at 134.3 eV, and 0.3 eV lower than the AlPO, at 133.0 eV. To our knowledge, there have been no reports of the P2p peak of P(III) phosphite using XPS. This downshift is an indication that our phosphorous might have retained the +3 oxidation state during deposition when using Me_3PO_3 as the phosphorous precursor and water as the reactant. More information can be obtained by comparing the P-peak shape of an AlPO film deposited using Me_3PO_3 precursor with the same peak on films deposited using $POCl_3$. In $POCl_3$, phosphorous is already in the +5 state. There are no significant differences in shape, only a shift of 0.5 eV (Fig. 8). This led us to believe that phosphorous in the films of this work retained the +3 oxidation state for LiPO, and AlPO uncertain. To confirm this, we performed FTIR analysis to search for the PO_4-signal at around 1200 cm^{-1} (Fig. 9). There is a significant difference in the lithium systems. Li_3PO_4 has a sharp PO_4 absorption at 1132 cm^{-1}, and this absorption is not present for Li_3PO_3, thus confirming that we do not have phosphate in our films. The peak at 870 cm^{-1} can be related to P-O stretch for P(III) phosphorous,[27] thus confirming that the oxidation state and the local structure of phosphorous are conserved during synthesis. The broad asymmetric peak at 1400–1600 cm^{-1} is still unaccounted. It overlaps with the carbonate signal range, but due to the low carbon content in the material, this is an unlikely conclusion. The AlPO system is not as clear-cut: The peak at 1220 cm^{-1} is shifted to 1200 cm^{-1} when going from $AlPO_4$ to $AlPO_3$. There is an additional peak at 610 cm^{-1} for $AlPO_3$, and the P-O peak at 890 cm^{-1} is more

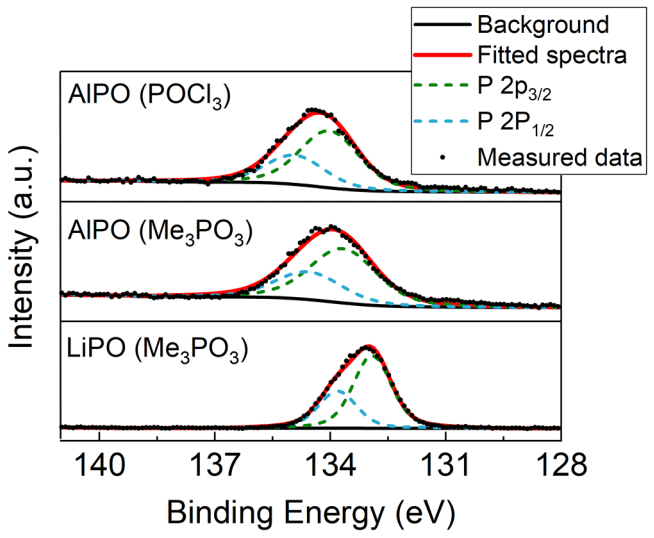

FIG. 8. Phosphorous P2p peaks from XPS analysis. The data were aligned to the adventitious carbon peak at 284.8 eV.

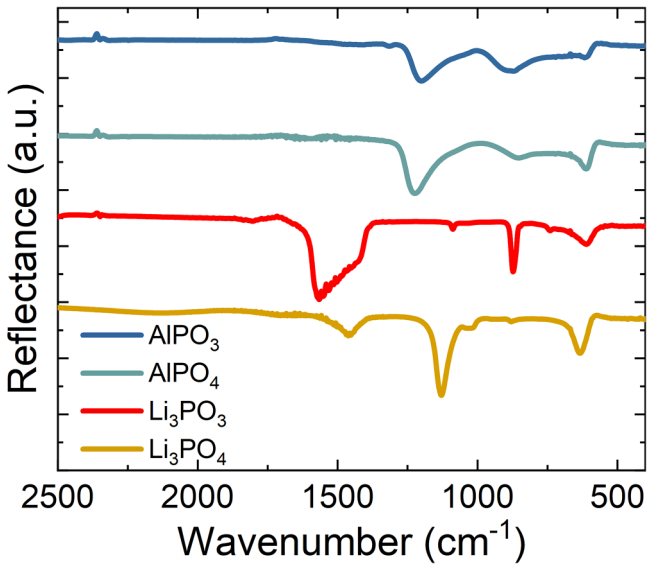

FIG. 9. Reflection FTIR of the LiPO and AlPO films, with comparisons to phosphate films deposited in the same reactor.

pronounced and a lot broader. Broad peaks from amorphous Al-O stretching can appear in this region; the $AlPO_3$ peak around 850 cm^{-1} can be assigned to isolated Al-O-Al sites, and downshift to around 870 cm^{-1} in $AlPO_4$ for similar clusters.[28] This hints at less ordering when going from phosphite to phosphate.

The surface topography of AlPO and LiPO films deposited at 225 °C was investigated by AFM and shows a highly textured surface for the LiPO films while the AlPO films are less rough, as seen in Fig. 10(a). The measured LiPO film is 25 nm thick with an RMS roughness of 4.7 nm. In addition, narrow pillars that are 30 nm higher than the area immediately surrounding the peaks are visible. Thin, crystalline pillars or spikes are the likely shape of the surface when particles form through reservoirs of hygroscopic Li (OH) formed during growth. Such particles may react further when exposed with air to form Li_2CO_3. There are visible drift effects in the LIPO image; however, the image still demonstrates the large surface roughness. The surfaces of the AlPO films were found to be compliant to the assumption of uniform films, with an RMS roughness of 0.1 nm and some smaller peaks that are up to 4 nm higher than the surrounding area [Fig. 10(b)]. The topography for both films is clearly different to those deposited by Hämäläinen *et al.*[9,13] for the same systems, using fully oxidized phosphorous precursors. Those films show larger features that indicate microcrystallinity. The crystallinity of their film is proven by XRD, unlike the films presented in this work, where all are x-ray amorphous; this is surprising when considering the LIPO AFM measurements. Some care must be taken with this comparison since Hämäläinen *et al.* used SEM for topographical analysis.

IV. DISCUSSION

Our investigations show that there are differences between phosphite and phosphate precursors. We observe increased reactivity for Me_3PO_3 as compared to using Me_3PO_4, where the latter requires a highly reactive coreactant for efficient deposition. FTIR analysis performed on the samples after deposition clearly indicates that phosphate is not present in Li_3PO_3 films. The phosphorous oxidation state is kept at +3 during the deposition. The AlPO analysis is not as clear, and the phosphate peak is visible in the FTIR spectrum but shifted by about 20 cm^{-1}. We see some peak shifts in both the FTIR and XPS data but not enough to give a clear indication of the phosphorous oxidation state for ALPO. If the product is indeed $AlPO_4$, something unknown must have been reduced in addition. Phosphates can form structures with varying degrees of polymerization, ranging from orthophosphates with Li_3PO_4 composition to chain structures with Li_3PO_3 composition. Extreme polymerization into P_2O_5 chains was not observed in this work.[29] By applying the possibilities of polymerization to the information in Table II, we can gain some insights into the film structure. The most interesting sample is the one characterized by TOF-ERDA, being less perturbed by surface carbon. The high oxygen content of the sample indicates an orthophosphate structure even when assuming that all carbon is in the form of carbonate. The AlPO system has even less phosphorous incorporated into the films than the LiPO system, too little to give $AlPO_4$ as the only product. For the AlPO film with the highest phosphorous content (AlPO 1:9),

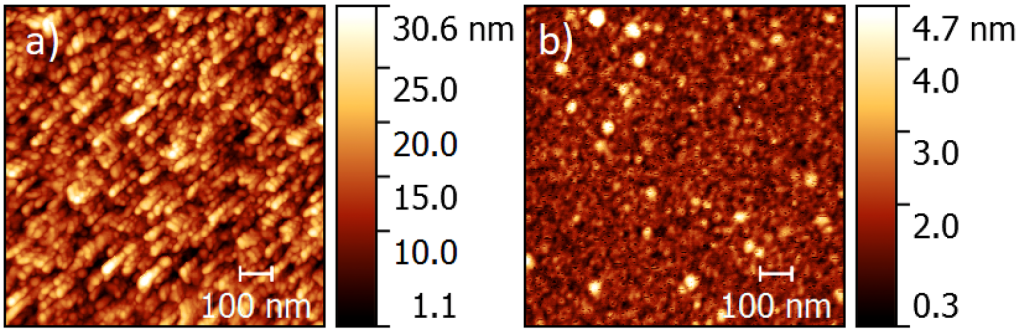

FIG. 10. Topography of LiPO films (a) and AlPO films (B) as measured by AFM.

the average formula is $Al_{2.1}PO_{5.5}$. By assuming $AlPO_4$ as the main product, the film must in addition contain 0.5 Al_2O_3. The average composition is close to the $Al_2PO_{5.5}$ previously reported by Meyers *et al.*,[6] based on Al-O_6 octahedra as reported by Saraswati *et al.*[30] This explanation leaves 0.2 Al unexplained. The other AlPO films synthesized in this work have even less phosphorous incorporated. The films synthesized using a phosphite precursor is otherwise similar to films synthesized with phosphate precursors, albeit with slightly different stoichiometries. This is an indication that Me_3PO_3 is a good phosphorous precursor in ALD.

V. CONCLUSION

We have shown the successful deposition of LiPO and AlPO using trimethyl phosphite as the phosphorous precursor. The trivalent phosphorous remained as P(III) during the deposition for the LiPO system, and probably also for the AlPO system, based on similar shifts in the XPS data. Trimethyl phosphite has properties that are preferable in ALD synthesis such as high vapor pressure and good reactivity. This precursor can enable further exploration of phosphorous based ALD synthesis. Triethyl phosphite did not produce any film and was discarded as an ALD precursor in these synthesis routes.

ACKNOWLEDGMENT

The authors gratefully acknowledge the Research Council of Norway (Grant Agreement Nos. Nano-MILIB, 143732 and Solib, 622304) for financial support.

DATA AVAILABILITY

The data that support the findings of this study are available from the corresponding author upon reasonable request.

REFERENCES

[1]H. O. Pastore, S. Coluccia, and L. Marchese, Annu. Rev. Mater. Res. **35**, 351 (2005).
[2]S. Kitagawa, R. Kitaura, and S.-i. Noro, Angew. Chem., Int. Ed. **43**, 2334 (2004).
[3]A. Gutierrez, N. A. Benedek, and A. Manthiram, Chem. Mater. **25**, 4010 (2013).
[4]M. Putkonen, T. Sajavaara, P. Rahkila, L. Xu, S. Cheng, L. Niinistö, and H. J. Whitlow, Thin Solid Films **517**, 5819 (2009).
[5]H. H. Sønsteby, E. Østreng, H. Fjellvåg, and O. Nilsen, Chem. Vap. Deposition **20**, 269 (2014).
[6]S. T. Meyers, J. T. Anderson, D. Hong, C. M. Hung, J. F. Wager, and D. A. Keszler, Chem. Mater. **19**, 4023 (2007).
[7]M. N. Getz, P.-A. Hansen, H. Fjellvag, and O. Nilsen, RSC Adv. **7**, 8051 (2017).
[8]S. M. George, Chem. Rev. **110**, 111 (2010).
[9]J. Hamalainen, J. Holopainen, F. Munnik, T. Hatanpaa, M. Heikkila, M. Ritala, and M. Leskela, J. Electrochem. Soc. **159**, A259 (2012).
[10]M. Nieminen, L. Niinistö, and R. Lappalainen, Microchim. Acta **119**, 13 (1995).
[11]A. Pettersen, V. Brei, V. Kaspersky, and N. Gulyanitskaya, React. Kinet. Catal. Lett. **50**, 415 (1993).
[12]O. Nilsen, H. Fjellvåg, and A. Kjekshus, Thin Solid Films **444**, 44 (2003).
[13]J. Hämäläinen, J. Holopainen, F. Munnik, M. Heikkilä, M. Ritala, and M. Leskelä, J. Phys. Chem. C **116**, 5920 (2012).
[14]T. Dobbelaere, A. K. Roy, P. Vereecken, and C. Detavernier, Chem. Mater. **26**, 6863 (2014).
[15]K. B. Gandrud, A. Pettersen, O. Nilsen, and H. Fjellvag, J. Mater. Chem. A **1**, 9054 (2013).
[16]W. Biqiong, L. Jian, S. Qian, L. Ruying, S. Tsun-Kong, and S. Xueliang, Nanotechnology **25**, 504007 (2014).
[17]G. Sauerbrey, Z. Phys. **155**, 206 (1959).
[18]M. Laitinen, M. Rossi, J. Julin, and T. Sajavaara, Nucl. Instrum. Methods Phys. Res., Sect. B **337**, 55 (2014).
[19]M. Putkonen, T. Aaltonen, M. Alnes, T. Sajavaara, O. Nilsen, and H. Fjellvag, J. Mater. Chem. **19**, 8767 (2009).
[20]E. Østreng, H. H. Sønsteby, T. Sajavaara, O. Nilsen, and H. Fjellvåg, J. Mater. Chem. C **1**, 4283 (2013).
[21]O. Nilsen, O. B. Karlsen, A. Kjekshus, and H. Fjellvåg, Thin Solid Films **515**, 4550 (2007).
[22]Y. B. Kim, Electrochem. Solid-State Lett. **3**, 346 (1999).
[23]V. Miikkulainen, O. Nilsen, M. Laitinen, T. Sajavaara, and H. Fjellvåg, RSC Adv. **3**, 7537 (2013); M. Putkonen, T. Sajavaara, L. Niinistö, and J. Keinonen, Anal. Bioanal. Chem. **382**, 1791 (2005).
[24]A. C. Kozen, A. J. Pearse, C.-F. Lin, M. Noked, and G. W. Rubloff, Chem. Mater. **27**, 5324 (2015).
[25]B. V. R. Chowdari, K. L. Tan, and W. T. Chia, Solid State Ionics **53**, 1172 (1992).
[26]A. T. Appapillai, A. N. Mansour, J. Cho, and Y. Shao-Horn, Chem. Mater. **19**, 5748 (2007).
[27]L. Daasch and D. Smith, Anal. Chem. **23**, 853 (1951).
[28]V. M. Bermudez, R. L. Rubinovitz, and J. E. Butler, J. Vac. Sci. Technol. A **6**, 717 (1988).
[29]É. Guille, G. Vallverdu, and I. Baraille, J. Chem. Phys. **141**, 244703 (2014).
[30]V. Saraswati, G. V. N. Rao, and G. V. Rama Rao, J. Mater. Sci. **22**, 2529 (1987).